

# Comparative analysis of Hydro-Station liquefaction potential: A case study

Claudine Nackers & Nouredine Ghlamallah

*Englobe Corp., Laval, Quebec, Canada*

Mourad Karray & Mahmoud N. Hussien

*Département de génie civil – Université de Sherbrooke, Sherbrooke, Québec, Canada*

Chekired Mohamed

*Hydro-Québec, Montréal, Québec, Canada*



## ABSTRACT

The comprehensive geotechnical investigation conducted by Englobe Corp. in 2015, as part of the construction of an extension of a hydroelectric station located in the Sorel-Tracy region, indicated the potential presence of three layers of liquefiable soils at certain depths. An additional specialized subsurface investigation for the liquefaction issue was conducted mainly to determine the shear wave velocity,  $V_s$  profiles of the deposits with three different methods; namely, the seismic piezocone, Multi-Modal Analyses of Surface Waves, MMASW and P-RAT laboratory tests. A series of cyclic shear tests using the TxSS seismic simulator were then carried out to characterize the dynamic properties of soil samples extracted from the site and reconstituted at the same in-situ density to assess their liquefaction potential. Based on both the experimental and the numerical comparative results, the soil deposit at the site is judged to be safe against liquefaction with an adequate margin of safety.

## RÉSUMÉ

L'étude géotechnique effectuée par Englobe Corp. en 2015 dans le cadre du projet d'agrandissement d'un poste hydroélectrique situé dans la région de Sorel-Tracy, a conclu qu'il y avait un risque de liquéfaction de trois couches situées à différentes profondeurs. Des investigations supplémentaires ont été menées pour déterminer les vitesses de cisaillements en utilisant trois méthodes, soit le sismocône, Multi Modal Analyses of Surface Waves, MMASW et des essais en laboratoires P-RAT. Ensuite, une série d'essais de cisaillement cycliques, TxSS, ont été effectués en utilisant un simulateur sismique pour caractériser les propriétés dynamiques des sols et évaluer leur potentiel de liquéfaction. Basé sur les résultats expérimentaux et numériques comparatifs, les sols du Poste Carignan ont été jugés sécuritaires contre la liquéfaction avec une bonne marge de sécurité.

## 1 INTRODUCTION

The project consisted of the extension of an existing hydroelectric station located in the Sorel-Tracy region. The general stratigraphy present on site is composed of:

- a very loose to compact sand deposit (SM) of a thickness varying between 7.0 and 9.3 m overlaying;
- a very loose to loose silty sandy deposit with clayey layers (ML/CL) of a thickness of about 25 m overlaying;
- a stiff to very stiff clay deposit (CL) overlaying; and
- the bedrock is at a depth estimated at 77 m.

Initially, a simplified liquefaction potential analysis based on the results of the Standard penetration Test (SPT) using Youd et al. (2001) approach and a dynamic analysis based on Cone Penetration Test (CPT) using Robertson et al. (1998) approach have concluded that most of the sand deposit and the silty sandy deposit have a high liquefaction potential.

Considering that the options for piles and soil improvement were not possible because of the thickness of the liquefiable deposits for the first option and the proximity of the existing structures for the second option, a more precise evaluation of the liquefaction potential has become necessary.

Although the dynamic approach is more accurate than the simplified approach, the full dynamic approach uses

stiffness and damping degradation curves as well as soil cycling resistance (CRR) from tests on soils not from the Eastern Canada region. In order to consider local soil conditions and properties, it was concluded that additional samples and laboratory tests were needed to further analyze the liquefaction potential.

In addition to presenting the specific study, this case study will present and compare three different methods to measure shear velocity.

The seismic piezocone is a widely used in-situ test and has the advantage of collecting data on a wide range of geotechnical parameters of the soils and the seismic shear velocities,  $V_s$ , simultaneously (Campanella and Stewart, 1992). However, in this case, the bedrock is located at about 77 m of depth and the system used could not reach that depth.

A Multi-Modal Analysis of Surface Wave, MMASW, line (Lefebvre and Karray 1998) was used to complete the  $V_s$  profile and determine the bedrock depth.

A P-RAT system was used (Karray et al. 2015a) in an oedometer cell to measure the  $V_s$  at different densities to reconstitute the remoulded samples in the laboratory at the same in-situ conditions.

The site-specific study to determine the liquefaction potential was done using the energy concept (Berril et Davis 1985, Karray et al. 2015b, and Polito et al. 2013).

To determine the dynamic parameters of the site's soils, cyclic triaxial simple shear tests, TxSS, (Chekired et

al. 2015, Kararay et al. 2015b) were done on the reconstituted samples and intact clay sample enclosed in an unreinforced rubber membrane. The test consists of a simple shear test at strain control in a drained triaxial cell. The cyclic stress ratio, the strain and the pore pressure are measured in real time during the test. The apparatus can apply cyclic or irregular strains to the sample.

## 2 GEOTECHNICAL PROPERTIES OF SOILS

The following tables and figures present an overview of the geotechnical properties of the tested soil samples. The soil samples were chosen based on the Standard Penetration Test  $N$  value  $N_{SPT}$  and Tip Resistance  $q_c$  (CPT) measured onsite.

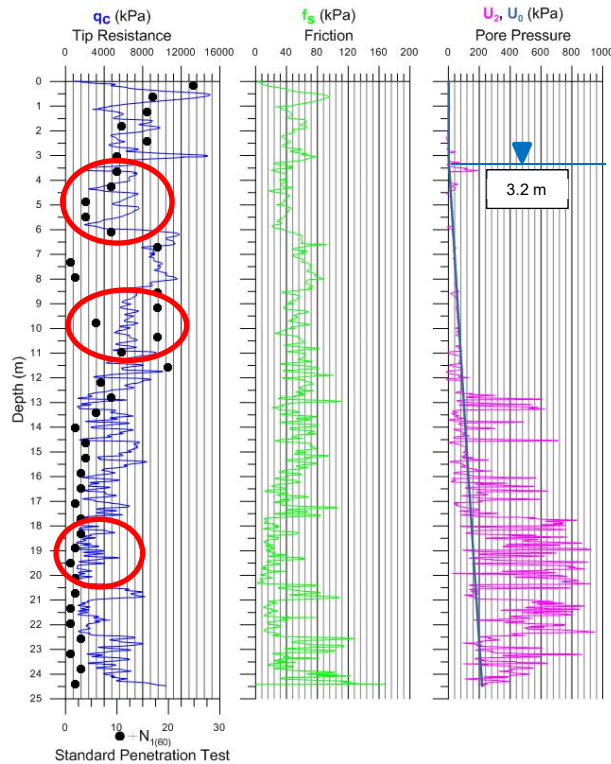


Figure 1. sCPT results. Circled in red are the targeted layers with the lowest  $N_{SPT}$ , and  $q_c$  measurements for the laboratory testing.

From a depth of 12.5 m, layered sandy silty soils was intercepted and thin clay layers can clearly be observed on the CPT results with precision of less than 10 mm. The clay layer was intercepted at a depth of 32.0 m and Shelby tubes were sampled. The plasticity index of the clayey soil varies between 8 and 11%, which indicates a low plasticity soil, the limit liquid varies between 0.85 to 1.5, which indicates high sensitivity of the clay. The layers with low strength and compactness are identified in Table 1.

Table 1. Density of tested soils

Sample	Depth (m)	$q_{t,mean}$ (kPa)	$N_{1(60)}$
CF-9	4.6 – 5.2	6300	4
CF-18	10.1 – 10.7	6200	4
CF-31	18.0 – 18.6	2850	3

Figure 2 presents the sieve analysis for the selected layers. The sample CF-9, obtained at a depth of 4.6 to 5.2 m, consists of a silty sand (SM). The samples CF-18 and CF-31, sampled at depths of 10.1 to 10.7 m and 18.0 to 18.6 m, respectively are very similar and consist of silty sand (SM) as well, but with a higher content in silt and fine sands. Table 2 presents the soil classification and physical parameters of the tested soils.

Table 3 presents the geotechnical parameters of the thin clay layers (CF-28) intercepted from 12.0 m and clay layer (CF-18 and CF-31) intercepted at 32.0 m.

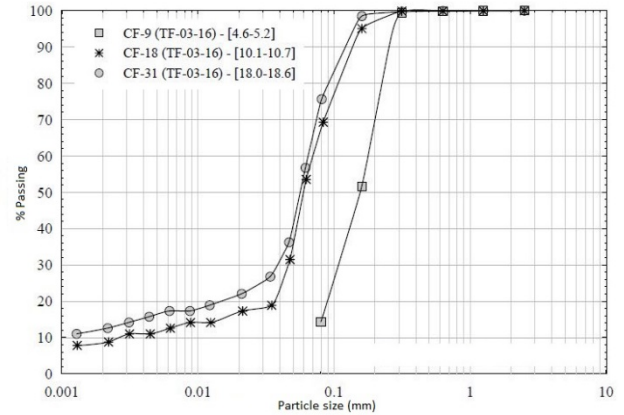


Figure 2. Sieve analysis of sand and silt soils. All three samples consist of silty sand (SM) with variable fine content.

Table 2. Physical properties of non-plastic tested soils

Sample	Depth (m)	Fines (%)	$D_{50}$ (%)	$C_u$	USCS
CF-9	4.6 – 5.2	14	0.15	2.45	SM
CF-18	10.1 – 10.7	69	0.061	28	SM
CF-31	18.0 – 18.6	76	0.056	56	SM

Table 3. Physical properties of clayey soils (CL)

Sample	Depth (m)	$W_n$ (%)	$W_L$ (%)	$W_P$ (%)	$I_P$ (%)	$I_L$
CF-28	16.2 – 16.8	31.0	27.0	19.0	8	1.5
CF-53	32.0 – 32.6	34.0	30.0	20.0	10	1.4
TM-56	34.0 – 34.6	29.7	31.3	20.3	11	0.85

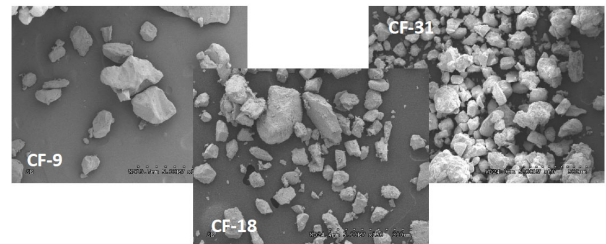


Figure 3. Grain shape of tested soils

Figure 3 presents the grain shape of the tested soils. The grains are very angular and micas minerals were

observed which indicates that the soils were not transported during their deposition. It is worth mentioning that particle shape as an inherent soil characteristic plays a significant role in liquefaction susceptibility of soils (Vaid et al. 1985; Hird and Hassona, 1990; Ashour and Norris 1999, Ashmawy et al. 2003).

### 3 COMPARING SHEAR WAVE VELOCITY METHODS

Three methods were used to measure shear wave velocity:

- Seismic piezocone, sCPT;
- Multi-Modal Analyses of Surface Wave, MMASW; and
- P-RAT laboratory measured Vs.

The measured in-situ velocities were compared to calculated velocities from Standard Penetration,  $N_{SPT}$ , values and corrected static cone tip resistance,  $q_t$  to validate the in-situ measurements (Figure 4).

For the Standard Penetration values, Wride et al. (2000) recommends using Eq. 1:

$$V_{s1} = 105 N_{1(60)}^{0.25} \quad [1]$$

Where  $V_{s1}$  is the shear wave velocity normalized with the vertical effective stress  $[SA1]$  and  $N_{1(60)}$  is the Standard Penetration values corrected for 60% of the energy. The measured  $N_{SPT}$  values were corrected using the Skempton (1986) corrections and the energy transfer ratio, ETR, measured from a SPT-Analyzer.

To convert the normalized shear wave velocity,  $V_{s1}$ , to standard shear wave velocity, Eq. 2 below was used:

$$V_s = \left( \frac{\sigma'_{v0}}{100} \right)^{0.25} V_{s1} \quad [2]$$

Where  $\sigma'_{v0}$  is the effective overburden pressure.

For the cone resistance,  $q_t$ , the relation from Perret et al. (2016) was used (Eq. 3):

$$V_s = 39 * q_t^{0.164} * z^{0.137} \quad [3]$$

To calculate the  $V_s$  with the cone resistance,  $q_t$ , the mean of the measured data of the layers were used.

The aberrant data at 2 m of depth for the seismic piezocone was not considered in the analysis.

The relation of Wride et al. (2000) is used to compare in-situ measured  $V_s$  values with those calculated from the measured  $N_{1(60)}$ . Similarly, the Perret et al., (2016) relation is used to compare in-situ measured  $V_s$  values with those calculated from measured  $q_t$  values.

The calculated  $V_s$  with the  $N_{1(60)}$  largely underestimates the shear wave velocity. This is common in saturated silty deposit as the  $N_{spt}$  values underestimate the rigidity of the soils. This indicates that using the  $N_{spt}$  values for the liquefaction analysis might be conservative. Furthermore, the relations developed are for sand deposits with  $D_{50}$  varying between 0.16 and 0.25.

The calculated  $V_s$  with the cone resistance data,  $q_t$ , fits the measured data very well.

The  $V_s$  is a function of several geotechnical parameters such as the void ratio, density, granulometry,

overconsolidation ratio, age, cementation, etc. (Hussien and Karray, 2015), which makes it an useful parameter to recreate, with high accuracy, the in-situ conditions of reconstituted samples tested under laboratory conditions. In addition, unlike penetration tests, which cannot be performed conveniently in laboratory and in field at all depths or in all soils, shear wave velocity offers to geotechnical engineers a promising alternative to penetration indexes to evaluate liquefaction resistance of sandy soils (Tokimatsu and Uchida 1990, Dobry and Abdoun 2011).

The P-RAT system was used in an oedometer cell to measure the  $V_s$  at different densities.

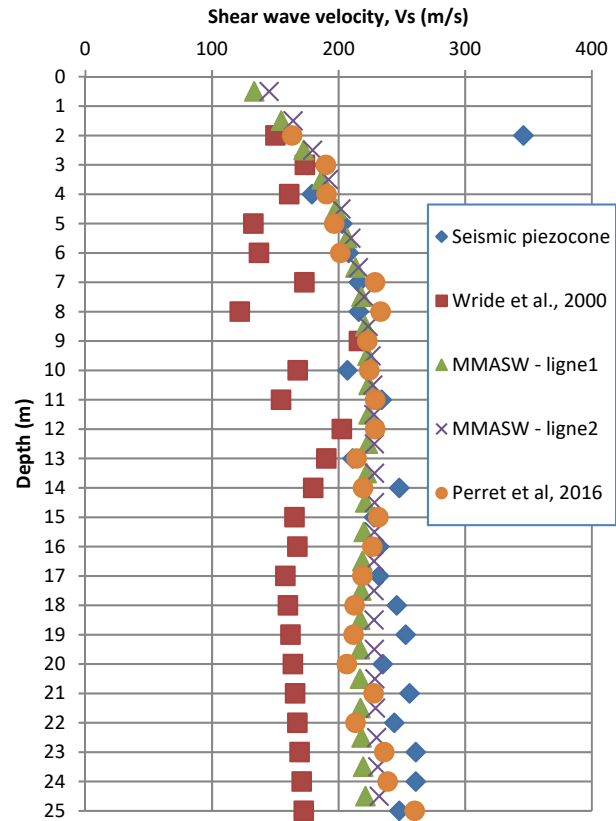


Figure 4. Comparison of in-situ measured shear velocity and theoretical velocities

The clay soil (TM-56) was retrieved from a Shelby tube. P-RAT tests were done on the intact samples (Figure 5).

Figure 6 presents the results of the P-RAT tests on the reconstituted sample CF-9 (4.6 – 5.2 m) at different densities.

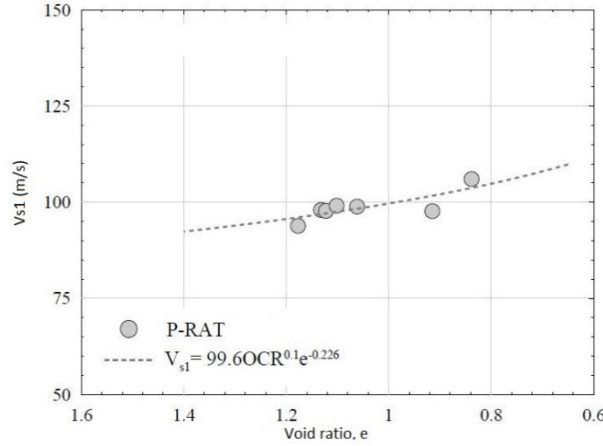


Figure 5. P-RAT test results for clay soil (TM-56)

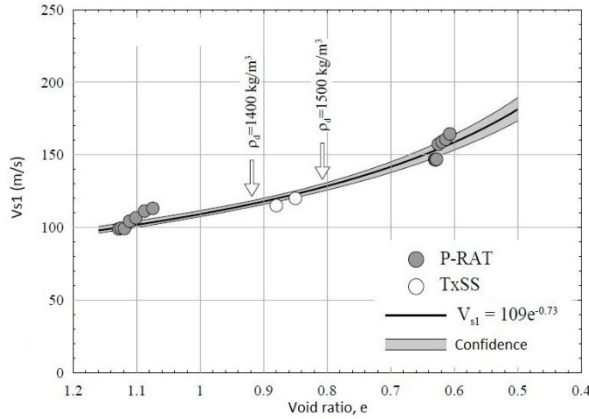


Figure 6. P-RAT test results for sand soil (CF-9)

For each of three sample, two densities were chosen to proceed the TxSS tests in accordance with  $V_s$  values obtained in the site: 1400 kg/m<sup>3</sup> and 1500 kg/m<sup>3</sup>; which corresponds to a density index of 20-30% and 40-45% respectively.

Table 4 compares the shear wave velocities measured in-situ and in the lab at different densities.

Table 4. Dynamic properties of tested soils

Sample	Depth (m)	$V_{s1}$ -in-situ	$V_{s1}$ -Lab 1400 kg/m <sup>3</sup>	$V_{s1}$ -Lab 1500 kg/m <sup>3</sup>
CF-9	4.6 – 5.2	227	110	125
CF-18	10.1 – 10.7	203	110	130
CF-31	18.0 – 18.6	212	115	130
TM-56	34.0 – 34.6	183		105

#### 4 ENERGY-BASED CONCEPT

This section presents the key concepts for the energy-based liquefaction analysis.

When using the conventional approach in total stress from Seed and Idriss (1970) implemented in software like

SHAKE2000, the dynamic properties are defined by the  $G/G_{max}$  degradation curve and the damping curve  $\lambda$ .

When using the energy-based concept, the dynamic properties are defined by the pore pressure ratio,  $R_u$ , and the stress-shear soil behavior.

Unlike the standard cyclic shear tests, DSS, the TxSS can measure the pore pressure ratio,  $R_u$ , directly instead of calculating it through empirical equations (Karray et al. 2015).

The pore pressure ratio,  $R_u$ , is a function of the normalized unit energy,  $W_s$ , the cyclic strain,  $\gamma$ , and the cyclic stress ratio, CSR (Polito et al. 2013).

The normalized unit energy,  $W_s$ , is the area of the hysteresis loop formed by the stress-strain relation during the cyclic shear test. The  $W_s$  can be calculated by integrating the area of the hysteresis loop as demonstrated in Figure 7. At each cycle, the soil degrades, the energy dissipates, and the  $R_u$  and CSR increase as shown in Figure 8.

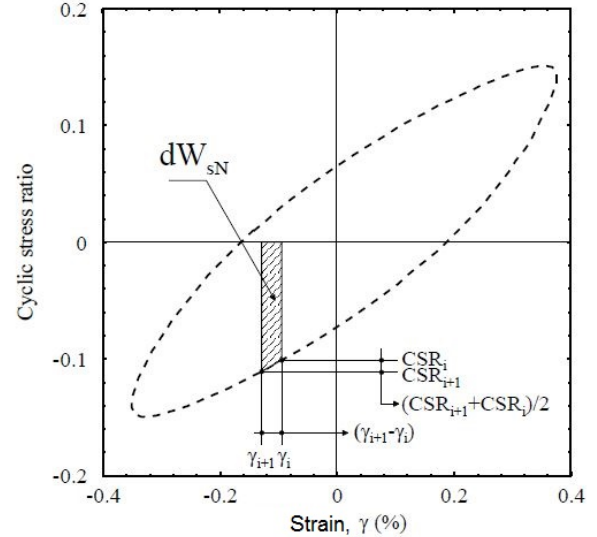


Figure 7. Normalized unit energy,  $W$ , determined from the hysteresis loop of degrading soils under seismic loading (taken from Karray et al. 2015b)

By using Berrill and Davis (1985) empirical equation modified by Karray et al (2015b), we can determine the  $R_u$  in function of the normalized  $W_s$  by using equation 4 for each soil sample tested.

$$R_u = \alpha_1 \left( \frac{W_s^{0.5}}{a} \right)^{\beta_1} \quad [4]$$

where  $a$ ,  $\alpha_1$  and  $\beta_1$  are constants.

The constants  $a$ ,  $\alpha_1$  and  $\beta_1$  are determined by calibrating equation 4 to the TxSS results to determine a specific  $R_u$  equation for each soil sample.

To model the stress-strain behavior, the software FLAC (Itasca, [www.itascacg.com/software/flac](http://www.itascacg.com/software/flac)) was used by building numerical hysteresis loops calibrated on the TxSS results.

Once the curves were calibrated, the numerical model was used to calculate the subsurface response to a design spectrum - compatible time history [SA2]Atkinson 2009).



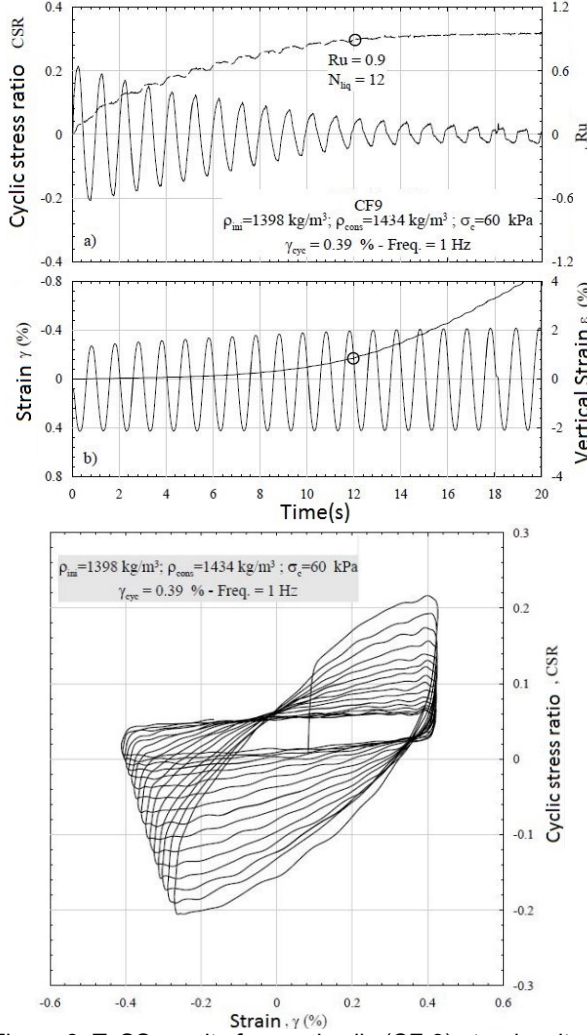


Figure 8. TxSS results for sand soils (CF-9) at a density of 1400 kg/m³

## 5 CYCLIC TRIAXIAL SIMPLE SHEAR TEST, TxSS AND VALIDATION OF NUMERICAL MODELS

The cyclic triaxial simple shear test, TxSS, consist of a simple shear test incorporated in a triaxial cell. The simple shear can be a cyclic strain or recreate a seismic strain based on real time histories. Since the cell is drained, the pore pressure ratio,  $R_u$ , can be measured directly. The pressure ratio is determined using equation 5:

$$R_u = \frac{\Delta u}{\sigma'_c} \quad [5]$$

where  $R_u$  is the pressure ratio,  $\Delta u$  is the pore pressure variation during the test, and  $\sigma'_c$  is the confinement pressure which is equivalent to the in-situ effective stress constraint,  $\sigma'_{v0}$ , of the sample.

After compacting and saturating the samples, they were sheared under a cyclic strain at 1 Hz. The number of cycles needed to liquefy a sample,  $N_{liq}$ , is when  $R_u$  reaches

0.9. At this ratio, the sample usually collapses or shows a well-defined shear band.

The tests were done on the same sample at two different densities,  $\rho_d = 1400 \text{ kg/m}^3$  and  $1500 \text{ kg/m}^3$  and at different shear strain,  $\gamma_{cyc}$ , varying between 0.27 and 0.80%.

### 3.1 Pore Pressure Ratio Equations

Figure 9 presents the pore pressure ratio,  $R_u$ , in function of  $W_s^{0.5}/a$ . These plots were used to calculate the constants  $\alpha$  and  $\beta$  and determine the samples' pore pressure ratio functions. Equations 6, 7, and 8, present the equations for samples CF-9, CF-18, and CF-31, respectively.

$$R_u = 0.26 \left( \frac{W_s^{0.5}}{a} \right) + 1.09 \left( \frac{W_s^{0.5}}{a} \right)^2 - 0.478 \left( \frac{W_s^{0.5}}{a} \right)^3 \quad [6]$$

$$R_u = 0.216 \left( \frac{W_s^{0.5}}{a} \right) + 1.325 \left( \frac{W_s^{0.5}}{a} \right)^2 - 0.65 \left( \frac{W_s^{0.5}}{a} \right)^3 \quad [7]$$

$$R_u = 0.248 \left( \frac{W_s^{0.5}}{a} \right) + 1.44 \left( \frac{W_s^{0.5}}{a} \right)^2 - 0.806 \left( \frac{W_s^{0.5}}{a} \right)^3 \quad [8]$$

The constant 'a' is a function of the shear strain,  $\gamma_{cyc}$ , and it depends on the compaction density,  $\rho_d$ . Figure 10 presents the plots of the constant in function of the shear strain for samples CF-9 and how the equation of the constant 'a' is determined from the TxSS results. Equations 9, 10, and 11 present the constant 'a' in function of the shear strain, for the samples CF-9, CF-18, and CF-31, respectively for compaction density,  $\rho_d = 1400 \text{ kg/m}^3$ .

$$a = 0.40 \gamma_{cyc}^{-0.98} \quad [9]$$

$$a = 0.85 \gamma_{cyc}^{-0.32} \quad [10]$$

$$a = 0.46 \gamma_{cyc}^{-0.92} \quad [11]$$

The same was done for the samples compacted to a density,  $\rho_d = 1500 \text{ kg/m}^3$ .

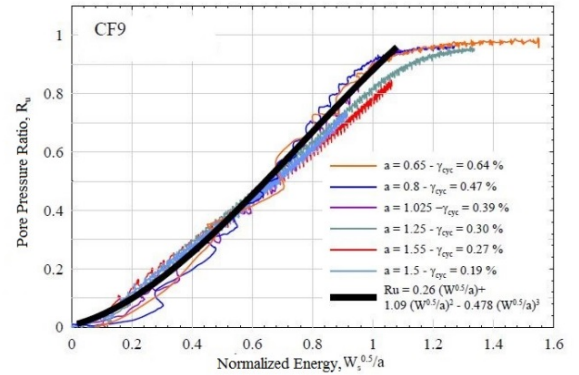


Figure 9. Pore pressure ratio,  $R_u$ , in function of the normalized unit energy,  $W_s^{0.5}/a$  for sample CF9 densified at  $\rho_d = 1400 \text{ kg/m}^3$

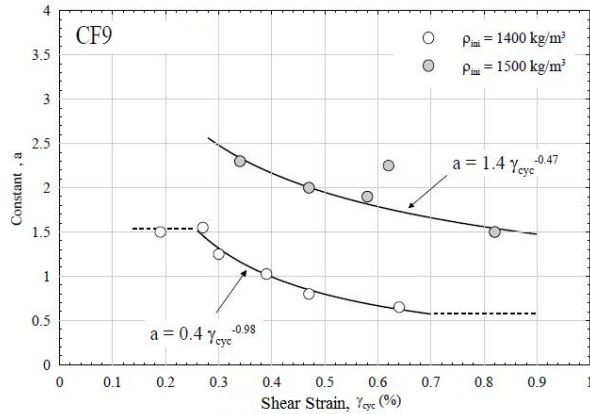


Figure 10. The constant 'a' is function of the shear strain,  $\gamma_{cyc}$  for the sample CF9 densified at  $\rho_d=1400 \text{ kg/m}^3$  and  $1500 \text{ kg/m}^3$ .

Using the pore pressure ratio,  $R_u$ , equations 6 to 8 and the constant 'a' equations, the test results could be simulated in FLAC. Figure 11 presents a comparison between the numerical model and the test results. The numerical data matches the test results indicating that the numerical model is well calibrated.

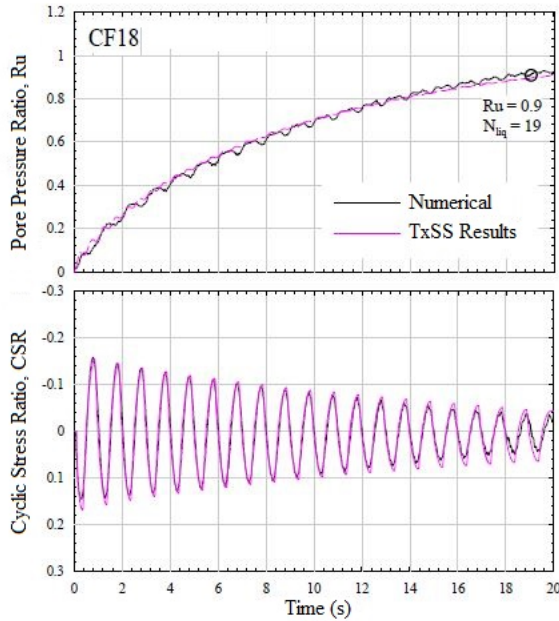


Figure 11. Comparison between the numerical data simulated in FLAC to the TxSS results using the  $R_u$  and constant 'a' equations.

### 3.2 Stress-Strain Hysteresis loops

The stress-strain hysteresis loops can be modeled in FLAC using the SIG4 function. Table 5 presents the constants used for the function.

Table 5. Constants used for the function SIG4 in FLAC to model the stress-strain hysteresis loops measured during the TxSS tests

Sample	a	b	$x_0$	$y_0$
CF-9	1.0	-0.50	-1.45	0.030
CF-18	1.0	-0.45	-1.45	0.045
CF-31	1.0	-0.45	-1.50	0.065
TM-56	1.0	-0.46	-1.50	0.065

Figure 12 compares the test results with the simulated hysteresis loops for sample CF9. This comparison was done for all the different strain tested and both of the density. There is a good match between the tested sample and numerical model results.

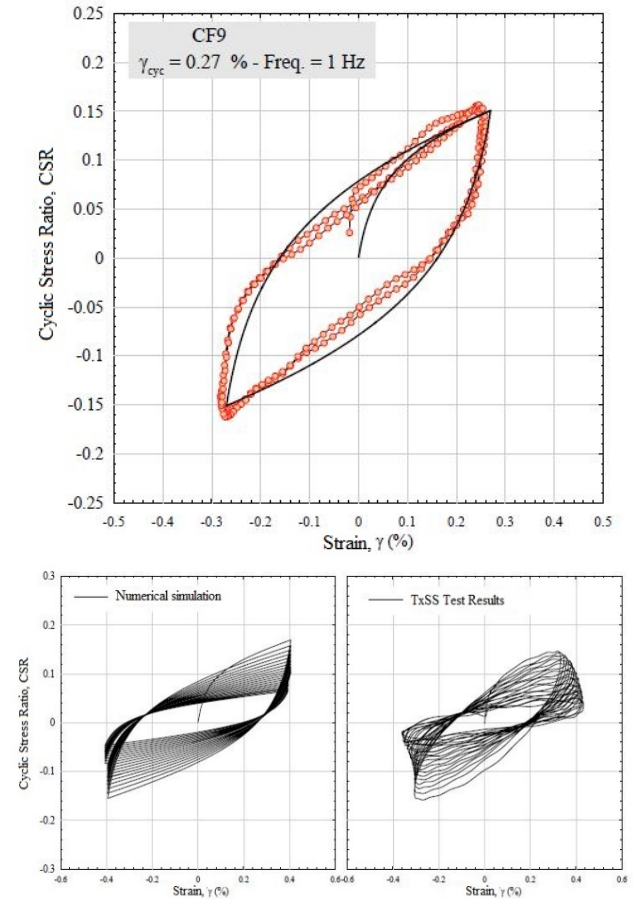


Figure 12. Comparison between simulated hysteresis loop in FLAC with the SIG4 function and test results for sample CF9 compacted at a density of  $1400 \text{ kg/m}^3$  and a shear strain of 0.27%.

## 4 SITE SPECIFIC STUDY

The TxSS results were used to analyze the liquefaction potential of the soils of the hydroelectrical station using the energy-based concept. FLAC, was used to model the dynamic response of the soil column based on the TxSS results with the equations and constants presented in Section 5.

The selection of time histories was done using the approach described by Atkinson (2009). Three ground motions mentioned in figure 13 were scaled to approximate

the design hazard spectrum of the site, UHS, of uniform hazard spectrum of a good quality bedrock based on the National Building Code of Canada NBCC 2010. Two time histories are synthetics taken from Atkinson's data base (<https://www.seisimotoolbox.ca/>). One is the 1985 Nahanni earthquake. Figure 13 presents the scaled spectral acceleration of the time histories used for this study.

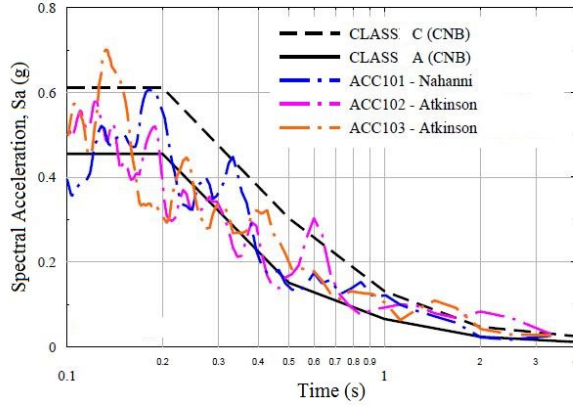


Figure 13. Response spectra of 3 different ground motions compatible with the design spectrum.

The factored time histories were applied at the bedrock to simulate the earthquake through the soil column and determine the soil degradation through time at different depth in the soil column.

With the TxSS results, the analysis is done in effective stress, since the pore pressure ratio,  $R_u$ , is calculated directly in the dynamic curves. Therefore, the shear modulus,  $G$ , can be adjusted during the simulation with equation 12 (Karray et al 2015b).

$$G = G_{ini}(1 - R_u)^\alpha \quad [12]$$

The constant ' $\alpha$ ' is calibrated with the TxSS test results. Figure 14, 15, and 16 present the results from the simulation at the depth of the soil samples CF-9 (4.6 - 5.2 m), CF-18 (10.1 - 10.7 m), and CF-31 (18.0 - 18.6 m).

The pore pressure ratio,  $R_u$ , for the three samples does not reach 0.9. Therefore, there is no liquefaction potential at these depths and with a good margin of safety. As mentioned in Section 2, these samples were chosen because they presented the lowest  $N_{SPT}$  and point resistance,  $q_c$ , measured in-situ for each soil layer encountered during the investigation campaign. We can conclude that the site does not present any liquefaction potential.

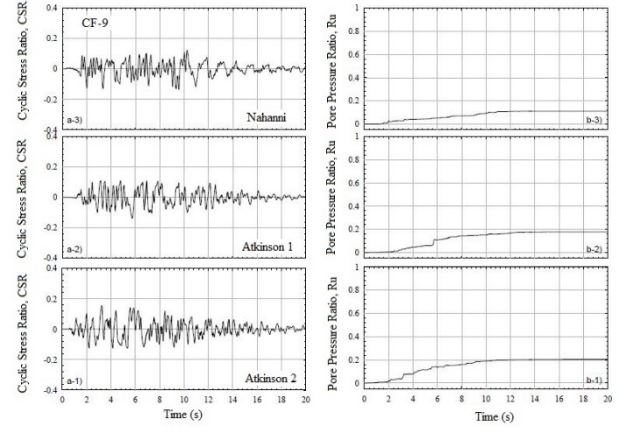


Figure 14. CSR and  $R_u$  results from FLAC simulation at CF-9 between depth 4.6 and 5.2 m for the three time histories

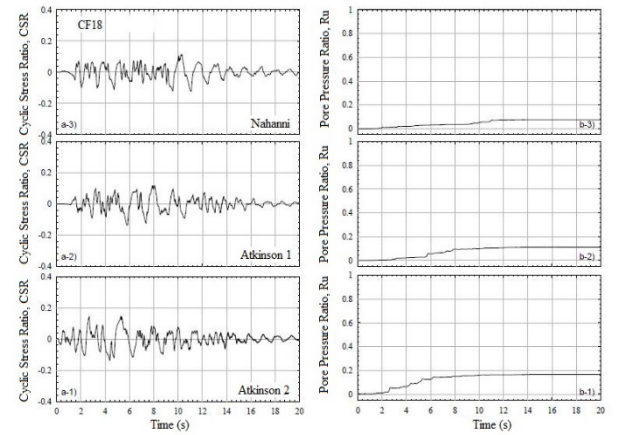


Figure 15. CSR and  $R_u$  results from FLAC simulation at CF-18 between depth 10.1 and 10.7 m for the three time histories

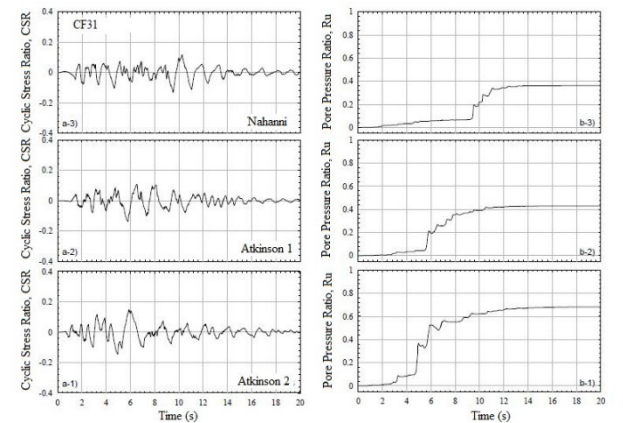


Figure 16. CSR and  $R_u$  results from FLAC simulation at CF-31 between depth 18.0 and 18.6 m

## 5 DISCUSSION AND CONCLUSION

The studied site presented a high liquefaction potential based on simplified and dynamic analysis approaches. A



complementary geotechnical investigation was done to measure the bedrock depth and a complete shear wave,  $V_s$ , profile.

The shear wave profile was validated using two in-situ methods, theoretical equations, and laboratory tests. It was observed that the theoretical shear wave using the  $N_{SPT}$  gave significantly lower shear waves than in-situ. The  $N_{SPT}$  were probably under-estimated due to pore pressure build up in the saturated silts. This was often observed with silty soils and therefore, the cone penetration test, CPT, is highly recommended for liquefaction analysis in these type of soils.

The in-situ shear wave velocities were used to re-constitute and compact the remoulded samples to the same densities as the measured in-situ.

A site specific dynamic analysis based on the energy concept using the TxSS results was performed on selected samples. The samples were selected in the very loose layers that present a liquefaction potential. The specific dynamic analysis concluded that the site presents no liquefaction potential.

To validate the numerical model, the test results were numerically modelled and compared to the laboratory test results. High correlation was observed between the numerical models and real test results for all samples.

## 6 REFERENCES

- Ashmawy, A.K., Sukumaran, B. and Hoang, V.V. 2003. Evaluating the Influence of Particle Shape on Liquefaction Behavior Using Discrete Element Modeling. *Proc. 13th Int. Off-shore and Polar Engineering Conference*: 542-549.
- Ashour, M., and Norris, G. 1999. Liquefaction and undrained response evaluation of sands from drained formulation. *Journal of Geotechnical & Geoenvironmental Engineering*, 125 (81): 649-658.
- Atkinson, G. M. 2009. Earthquake time histories compatible with the 2005 National building code of Canada uniform hazard spectrum. *Canadian Journal of Civil Engineering*, 36(6): 991-1000.
- Berrill, J. B., & Davis, R. O. 1985. Energy dissipation and seismic liquefaction of sands: revised model. *Soils and Foundations*, 25(2): 106-118.
- Campanella, R. G., & Stewart, W. P. 1992. Seismic Cone Analysis Using Digital Signal Processing for Dynamic Site Characterization. *Canadian Geotechnical Journal*, 29(3): 477-486.
- Chekired, M., Lemire, R., Karray, M., & Hussien, M. N. 2015. Experiment setup for simple shear tests in a triaxial cell: TxSS. *Proceedings of the 68th Conference of the Canadian Geotechnical Society*, Quebec City. Paper No. 365.
- Dobry, R., and Abdoun, T. 2011. An investigation in to why liquefaction charts work: A necessary step toward integrating the states of art and practice. *Proc., 5th Int. Conf. on Earthquake Geotechnical Engineering*, Chilean Geotechnical Society, Santiago, Chile, 13-44.
- Hird, C.C., and Hassona, F.A.K. 1990. Some factors affecting the liquefaction and flow of saturated sands in laboratory tests, *Engineering Geology* 28 (1-2): 149-170.
- Hussien, M. N., & Karray, M. 2015. Shear wave velocity as a geotechnical parameter: an overview. *Canadian Geotechnical Journal*, 53(2): 252-272.
- Idriss, I. M., & Seed, H. B. 1970. Seismic response of soil deposits. *Journal of Soil Mechanics & Foundations Div.*, 96(2): 631-638.
- Karray, M., Ben Romdhan, M., Hussien, M. N., & Éthier, Y. 2015a. Measuring shear wave velocity of granular material using the piezoelectric ring-actuator technique (P-RAT). *Canadian Geotechnical Journal*, 52(9): 1302-1317.
- Karray, M., Hussien, M. N., & Chekired, M. 2015b. Evaluation of compatibility between existing liquefaction charts in Eastern regions of North America. In *68th Canadian Geotechnical Conference*. Québec, Canada.
- Khashila, M., Hussien, M. N., Karray, M., & Chekired, M. 2015. Evaluation of equivalent cycle liquefaction concept based on TxSS test results. *GeoQuebec Conference*, Quebec, Canada.
- Lefebvre, G., & Karray, M. 1998. New developments in in-situ characterization using Rayleigh waves. *Proceedings of the 51st Canadian Geotechnical Conference*, Edmonton, Alta: 4-7.
- National Building Code of Canada, 2010. [National Research Council of Canada. Canadian Commission on Building and Fire Codes](#), vol. 1, p. 232; vol. 2, p. 971
- Perret, D., Charrois, E., & Bolduc, M. 2016. Shear Wave Velocity Estimation from Piezocone Test Data for Eastern Canada Sands (Quebec and Ontario)—Extended Version with Appendices. *Geological Survey of Canada*.
- Polito, C., Green, R. A., Dillon, E., & Sohn, C. 2013. Effect of load shape on relationship between dissipated energy and residual excess pore pressure generation in cyclic triaxial tests. *Canadian Geotechnical Journal*, 50(11): 1118-1128.
- Robertson, P.K. and Wride, C. E. (1998). Evaluation of Cyclic Liquefaction Potential using the Cone Penetration Test. *Canadian Geotechnical Journal*, Ottawa, 35(3), 442-459.
- Skempton, A. W. 1986. Standard penetration test procedures and the effects in sands of overburden pressure, relative density, particle size, ageing and overconsolidation. *Geotechnique*, 36(3): 425-447.
- Tokimatsu, K. and Uchida, A. (1990). Correlation between liquefaction resistance and shear wave velocity. *Soils and Foundations*, 30(2): 33-42.
- Vaid, Y.P., Chern, J.C., and Tumi, H. 1985. Confining pressure, grain angularity, and liquefaction. *Journal of Geotechnical Engineering*, 111 (10): 1229-1235.
- Wride, C. E., Robertson, P. K., Biggar, K. W., Campanella, R. G., Hofmann, B. A., Hughes, J. M., & Woeller, D. J. 2000. Interpretation of in situ test results from the CANLEX sites. *Canadian Geotechnical Journal*, 37(3): 505-529.
- Youd, T. L. et al. (2001), Liquefaction Resistance of Soils: Summary Report from the 1996 NCEER and 1998 NCEER/NSF Workshops on Evaluation of Liquefaction Resistance of Soils, *Journal of Geotechnical and Geoenvironmental Engineering*, October 2001: 817-833.